The Oceanic Response to Winds in the Antarctic Sea Ice Loss at the end of the 1970s

AUTHORS:

Feba F

Hugues Goosse

Pierre-Yves Barriat

François Massonnet

Affiliation: Earth and Climate Research Center, Earth and Life Institute, Université catholique de Louvain, Louvain-la-Neuve, Belgium

Correspondance: *feba.francis@uclouvain.be;* ORCID: 0000-0002-1917-3679

The Oceanic Response to Winds in the Antarctic Sea Ice Loss at the end of the 1970s

Feba F, H Goosse, P-Y Barriat, F Massonnet

Earth and Life Institute, Université catholique de Louvain, Louvain-la-Neuve, Belgium

Abstract

The sea ice extent (SIE) in the Southern Ocean experienced a substantial decline in the late 1970s, although less pronounced than the one observed in 2016. Though several studies explain the decline since 2016, the 1970s drop is critical in understanding the long-term variability of SIE. To investigate the underlying mechanisms for this decline, we conducted wind stress-forced multi-ensemble experiments using the general circulation model EC-Earth3 with constant pre-industrial CO_2. Using this anomaly-nudging technique, we reproduce the drop during the late 1970s, despite the control (no-nudging) run showing no such trend. The loss in SIE expresses spatial heterogeneity across different sectors of the Southern Ocean, with the maximum absolute loss occurring the King Hakon sector, followed by the Weddell Sea and Indian Ocean sectors. The loss of SIE co-occurred with an increase in temperature and salinity at the surface. Our analysis shows that this loss of SIE can be attributed to wind-driven oceanic twofold responses. 1) During the late 1970s, the wind stress curl was anomalously negative, driving a stronger Ekman upwelling, bringing salt and warmer water from the subsurface to the surface. 2) The winds shifted to a stronger phase during the same period, influencing the vertical mixing, inducing a deeper mixed layer and the entrainment of warmer and saltier water at depth in the mixed layer. This study highlights the importance of winds in driving ocean processes and thereby influencing the interannual variability of SIE in the Southern Ocean. Our results finally indicate that the late 1970s rapid sea ice loss event shares several characteristics with the recent post-2016 retreat, including a significant surface salinification despite substantial sea ice loss, suggesting that common mechanisms might be at play between the two periods and thus providing an insightful analogy to understand the current decline.

1. Introduction

The Southern Ocean sea ice is a large-scale, dynamic entity that acts as a barrier between the oceanic layer underneath and the atmosphere above, modulating the thermal, moisture, momentum and gaseous fluxes (Goosse & Fichefet, 1999; Rintoul, 2018; Schroeter, 2025). Over the past decade, the Southern Ocean sea ice extent (SIE) has received a surge in interest owing to its puzzling behaviour. For almost four decades, the SIE showed a slightly positive trend from 1979 to 2015 despite warming trends across nearly the entirety of the globe (Armour et al., 2016; Hobbs et

al., 2016; Parkinson, 2019; Thomas et al., 2015). This period was followed by the alarming SIE drop in 2016 (Meehl et al., 2019; Turner et al., 2017) and subsequently in 2023 and 2024 (Roach & Meier, 2025), marking a shift from the earlier observed upward trend to a pronounced low-extent regime (Fogt et al., 2022; Hobbs et al., 2024; Purich & Doddridge, 2023; Abram et al., 2025).

Several studies have proposed different mechanisms that, individually and collectively, with varying degrees, have possibly contributed to these drops in SIE, with atmospheric circulation clearly playing a dominant role. In particular, variations in the strength of the Amundsen Sea Low (ASL) contributed to the SIE loss by modifying atmospheric heat transport and sea ice transport (Turner et al., 2017; Jena et al., 2024; Wang et al., 2024). There were also some influences from the tropics, i.e., the extreme El Niño of 2015 (Stuecker et al., 2017), with a weaker impact related to the 2023 ENSO conditions (Espinosa et al., 2024), or a Rossby wave teleconnection from the tropical Indian Ocean (Purich & England, 2019). The positive phase of the zonal wave number three (ZW3) is also reported to have influenced the early melting and the rapid decline in SIE in 2016 due to an anomalous atmospheric southward heat transport (Schlosser et al., 2018).

Such wind circulation changes explain the majority of the interannual variability patterns and trends through both dynamic and thermodynamic effects across different regions of the Southern Ocean (Raphael, 2007; Lefebvre and Goosse, 2008; Massom et al., 2008; Holland and Kwok, 2012; Hosking et al., 2013; Raphael and Hobbs, 2014; Matear et al., 2015). However, the role of the ocean is also important, providing a preconditioning that could amplify the response to the atmospheric perturbations and feedbacks that prolong the influence of this perturbation. A warmer ocean causes delayed ice growth, and so a thinner ice ice pack on average, which in turn can melt earlier and more easily during the next season. In this framework, the subsurface warming observed before 2016 has been considered as an important element explaining the post-2016 shift in sea ice extent (Lecomte et al., 2017; Meehl et al., 2019; Zhang et al., 2022; Hobbs et al., 2024; Purich & Doddridge, 2023). The negative decadal trend of wind stress curl (WSC) associated with the positive phase of the Southern annular mode (SAM) caused an Ekman suction that induced warming in the Southern Ocean and contributed to the 2016 low SIE (Meehl et al., 2019; Zhang et al., 2022). In addition to this impact on the upwelling of warm water, stronger westerlies can also transport colder Antarctic surface water northward or reduce the horizontal heat transport in some sectors, driving sea ice expansion. Modifying the stratification of the water column and the vertical exchanges affects the winter ice thickness and SIE (Lecomte et al., 2017; Himmich et al., 2024; Spira et al., 2025). Based on an analysis of 110,000 hydrographic profiles, Spira et al. (2025) identified a thinning of the winter water layer between 2005 and 2015, which forms below sea ice in

winter and is sustained in summer below the mixed layer as a water layer at near-freezing temperatures. As this layer limits the exchanges between the warmer waters at depth and the surface, the consequent thinning reduces the strength of the barrier. Additionally, strong winds in 2015 were able to induce a large transport of heat from depth to the surface, contributing to the observed shift in SIE after 2015.

Many studies have been devoted to the shift in sea ice extent after 2015, but the lack of long and homogenous data records for SIE is a constraining factor in understanding the possibility of the occurrence of such sea ice loss events predating the satellite era from 1979. Nevertheless, several sea ice reconstructions based on various indirect climate records are available, although not without limitations (de la Mare, 2009; Dalaiden et al., 2021; Fogt et al., 2022; Goosse et al., 2024). These reconstructed longer datasets are essential in studying long-term trends or multidecadal variability in the sea ice, for example, the sector-wise variability of the sea ice edge in the Southern Ocean (Yang et al., 2021) or the influences of tropical drivers (Dalaiden et al., 2024). Recently, a multi-variate spatial reconstruction for the period 1958 to 2023 shows a loss of SIE of the order of 0.5 million km^2 in the Southern Ocean in the late 1970s (Goosse et al., 2024). Using a Bayesian reconstruction, another study also notes the probability of exceptionally low SIE in the Southern Ocean during the late 1970s (Raphael et al., 2025).

Though the reconstructions establish the presence of an earlier sea ice loss predating the satellite era, the mechanisms leading to this loss have not been explored in detail, necessitating a further detailed study. The analysis of the atmospheric circulation in the 1970s suggests a triggering role of the atmospheric circulation as observed during the post-2015 decrease (Goosse et al., 2024), but the oceanic contribution is more uncertain. The ocean has likely integrated the atmospheric forcing, prolonging the effect of the atmospheric anomalies; however, it is unclear if the ocean has only this relatively passive role or a more active one in the event. In the present study, we thus look at the potential role of the response of the ocean to wind changes and whether it could be the inception of this loss of SIE in the Southern Ocean towards the end of the 1970s.

In order to understand this potential role of ocean dynamics, we use here an Earth system model (ESM) to simulate the sea ice loss at the end of the 1970s. Recent studies have shown that when the winds are nudged in the atmosphere towards observations in an ESM, the model is able to follow some of the key characteristics of the observed changes in SIE (Blanchard-Wrigglesworth et al., 2021; Roach et al., 2023). This approach could have been applied here to try to reproduce the shift in sea ice extent at the end of the 1970s. However, the wind nudging modifies atmospheric heat

transport as well as the fluxes at the atmosphere-ocean-ice interface. It is thus impossible to disentangle the direct effect on sea ice of those imposed changes in the atmosphere from the response of the ocean. We have thus applied a different methodology in which we only perturb the wind stress at the surface based on observed winds. This modifies the oceanic circulation, which in turn influences the SIE and the atmosphere. With this experimental design, any change in the SIE must have its origin first in the ocean, allowing us to determine if modification of the oceanic state can explain a significant part of the SIE shift at the end of the 1970s. This approach also helps us to single out the role of dynamical factors, since the thermodynamical factors (large-scale atmospheric advection) are by design left unchanged.

2. Methods

2.1 Model Description

In this study, we carried out simulations using the European Community Earth System Model (EC-Earth; Döscher et al., 2022). The EC-Earth is a fully coupled atmosphere-ocean-ice model. The atmospheric component of EC-Earth is the Integrated Forecast System (IFS) from the European Centre for Medium-Range Weather Forecasts (ECMWF), cycle CY36R4. The atmospheric grid is the IFS standard resolution (T255L91), with approximately 80 km grid spacing and 91 vertical levels. The oceanic component is the Nucleus for European Modelling of the Ocean version 3.6 (NEMO; Madec and the NEMO team, 2015), with the Louvain-la-Neuve Sea Ice Model (LIM, version 3; Vancoppenolle et al., 2012; Rousset et al., 2015). The ocean-sea ice coupled NEMO3.6-LIM3 is used at 1^{o} resolution on the standard ORCA1 configuration with 75 vertical levels. The atmosphere and ocean-sea ice are coupled using the Ocean Atmosphere Sea Ice Soil coupler version 3 with the Model Coupling Toolkit (OASIS3-MCT). Our version, EC-Earth 3.3.3.2 is thus very similar to the one used for Coupled Model Intercomparison Project phase 6 (CMIP6), EC-Earth 3.3 (Döscher et al., 2022).

2.2 Experimental Setup

Our experiment is designed to force the model with monthly wind stress anomalies from ECMWF Reanalysis version 5 (ERA5, Hersbach et al., 2023). These anomalies are estimated compared to the mean seasonal cycle computed over the period 1960-2022. Perturbing with monthly anomalies instead of daily or hourly anomalies eliminates strong skewing due to extreme weather events. We modify the surface boundary conditions in NEMO during the coupling stage by adding wind stress perturbations to the value transferred from IFS by the coupler, consistently perturbing the model at all time steps. Therefore, the atmosphere can only be perturbed through the effect of the ocean,

removing the direct atmospheric influences from obfuscating any potential signal coming from the ocean.

To begin with, we carried out a control run (EC-CTL) with the standard configuration of the model, as a reference that will be compared to our perturbed experiments for assessing the impact of the wind forcing. All our simulations are run with prescribed CO_2, employing the constant pre-industrial conditions as defined for the CMIP6 (Eyring et al., 2016). Such simulations without anthropogenically induced forcings help differentiate the natural internal variability of the model climate system and identify the direct effect of the wind stress perturbation. We then carry out six ensemble members forced with identical wind stress anomalies. The ensemble members are all initialised in 1960 from conditions in EC-CTL selected at a consecutive interval of 10 years, starting in year 110 of this simulation. This indicates an effective spin-up time of at least 110 years for each ensemble member, a sufficient time scale for reaching a steady state within the upper ocean (not shown here). Each of the ensemble members (ECN1-ECN6) runs from 1960 to 2022. The different initial states are integral in separating the role of internal variability, due to differing phases of various climate modes, from the effect of the wind stress perturbation. We use the same wind stress forcing for all ensemble members. For our analysis, we calculate the ensemble mean (EnsMean) from the six ensemble members.

All the ensemble members and the control run have a robust and consistent seasonality for the Southern Ocean sea ice extent (SIE), comparable to that of the CMIP6 simulations (Roach et al., 2020). For each ensemble run, from 1960 to 2022, the mean seasonal cycle has a summer minimum of ~2 million km^2 in February and a winter maximum of ~19 million km^2 in September (Supplementary Figure 1). The monthly bias or the difference between monthly climatological SIE in EnsMean when compared with observational data from NSIDC (DiGirolamo et al., 2022) is on the scale of ~0.1 million km^2, with the least bias in October (0.025 million km^2) and the maximum bias in May (-0.277 million km^2). The standard deviation across the ensemble members has been calculated for each year (Supplementary Figure 2), with a mean of 0.41 million km^2 over the total period, 1960-2022. The coefficient of variation (ratio of standard deviation to mean), which indicates the spread of the ensemble members, for the same period, is 4.28%.

3. Results

3.1 Evolution of the Southern Ocean SIE

The evolution of the Southern Ocean SIE anomalies from our EC-Earth simulations is shown in Figure 1. As expected, the interannual variability of the EC-CTL diverges from the individual

ensemble members and the ensemble mean (EnsMean). However, all the wind stress forced simulations display similar multidecadal variability, and all the ensemble members are able to capture the observed drop (Goosse et al., 2024) in SIE at the end of the 1970s. By contrast, the EC-CTL experiment displays no such trend, suggesting that it is driven by the wind stress anomalies imposed in the perturbed experiments. The total SIE from the EnsMean, in the Southern Ocean, shows a steady increase in annual mean of over 1 million km^2 from 1960 (10.4 million km^2) to the mid-1970s (11.3 million km^2 in 1976), followed by a loss of about 12% during the next decade (9.3 million km^2 in 1990). A similar pattern of an increase and a subsequent decline in the late 1970s is apparent in the King Hakon and Weddell Sea sectors. The Indian Ocean sector had a decreasing SIE trend during the same period, although no increase was evident before the loss. The Amundsen-Bellinghausen seas show a very low decline in SIE, whereas the Ross Sea sector has no discernible trend throughout the run duration. The wind stress forced simulations (EnsMean) also show a SIE minimum in 2016, but we will not investigate in more detail this smaller drop and will focus on the clearer and larger signal at the end of the 1970s.

3.2 The Southern Ocean before and after the Sea ice loss

The period of maximum SIE extent in the EnsMean was in the late 1970s, and the subsequent minimum extent occurred during the early 1990s. We thus selected two periods, the period of maximum extent before the loss from 1976 to 1980 (pre-loss), and the subsequent minimum extent from 1990 to 1994 (post-loss), to compare and identify contrasting patterns (Supplementary Figure 3). From the EnsMean, the difference between the pre-loss (1976-1980) and post-loss (1990-1994) periods indicates a decrease of 1.28 million km^2 of SIE across the total Southern Ocean, with the ensemble members ranging from a minimum loss of 0.8 million km^2 to a maximum of 1.54 million km^2.

The loss of mean sea ice extent, which can be noticed as negative anomalies in sea ice concentration, almost everywhere except in the north of the Ross Sea (Figure 2). Sector-wise in the EnsMean, the SIE loss is more pronounced in King Hakon, the Weddell Sea and the Indian Ocean sectors. The Weddell Sea lost 0.36 million km^2 (Ensemble range: 0.18 million km^2 to 0.54 million km^2), the King Hakon Sector lost 0.4 million km^2 (Ensemble range: 0.27 million km^2 to 0.66 million km^2), and the Indian Ocean sector lost 0.23 million km^2 (Ensemble range: 0.07 million km^2 to 0.38 million km^2) of SIE, which contributed to 28.2%, 38.6% and 18% respectively to the total loss of SIE in the Southern Ocean. These sectors also had a large contribution to the loss, as identified in the reconstruction of Goosse et al. (2024).

All the ensemble members consistently show losses of varying magnitudes in all sectors in the Southern Ocean except for the Ross Sea, where the members differ and are non-conforming about an increase or decrease (Supplementary Figure 4). However, the maximum loss of SIE is observed over the region from 55^0S to 70^0S and from 50^0W to 30^0E, the Eastern Weddell Sea (EWS) sector (Figure 2). The EWS, in the EnsMean, lost 0.8 million km^2 of SIE in a decade compared to the pre-loss period. The SIE loss from the EWS sector contributed to about 63% of the total loss in SIE in the entire Southern Ocean during the same period. We then examine other oceanic parameters to understand the causes for this sea ice loss over the EWS region.

Unsurprisingly, the sea surface temperature (SST) difference fields reveal a warming over the EWS sector and more generally in all the sectors where SIE decreases (Figure 3a). The ocean temperatures from the surface to 100m depth have also shown a warming over the EWS sector during the same decade. Contrastingly, between the depths of 100m and 500m, the ocean temperatures show a relative cooling during this period (Figure 3c). The surface-to-subsurface contrast in warming/cooling is prominent in the EWS sector, with the warming at the surface shifting to a cooling below 100m depth. In some other regions, the cooling or warming tendency persists in the same phase from the surface to the deeper layers. In the larger Ross Sea Sector, between 180 and 120^0W, the cooling from the SST extends to the deeper layers. This is also the region of increased SIE during the late 1970s (Figure 2, Supplementary Figure 5). In the Amundsen-Bellingshausen Seas, the surface warming extends to the deeper layers.

During the same period, the mixed layer depth (MLD) also underwent several changes. The MLD deepened in the post-loss period relative to the pre-loss period over most of the Southern Ocean, though a shallowing of the MLD can be noticed in the western Weddell Sea, close to the Antarctic Peninsula (Figure 4a). In the EWS sector, the MLD increase coincides with the loss of SIE (Supplementary Figure 6).

The increase in MLD co-occurred with a simultaneous rise in surface salinity. The differences in the vertical profiles of temperature and salinity over the EWS sector show an increase in both parameters at the surface (Figure 4b). The salinity showed a difference between the two periods that increased gradually upwards from above 100m with a difference of 0.15 psu at the surface; however, there was no discernible difference in salinity below the 100m depth. Meanwhile, the temperature difference showed a steep decreasing difference between the two periods with a difference of 0.45˚C at the surface to about 100m depth where the temperature decreased by 0.13˚C.

Below the depth of 100m, the temperature difference decreases gradually with depth, showing a contrasting surface warming and subsurface cooling.

The increase in salinity in the Southern Ocean could be due to several factors. Freezing and melting of sea ice exert a strong control on oceanic surface salinity. However, during the late 1970s, the SIE decreases should have freshened the surface while our results are in contrast to this showing the salinity increasing simultaneously with decreasing SIE. Furthermore, there is very little difference in horizontal ocean current during the pre-loss or post-loss periods (Supplementary Figure 7). This rules out the hypothesis of horizontal advective supply of salts from other regions. Conclusively, the other remaining source of salinity is from below the surface. The increase in temperature along with salinity at the surface from the post-loss period compared to the pre-loss period also implies a supply from below as subsurface is warmer and saltier.

Considering the experimental design, forcing the ocean with the wind stress anomalies, the role of winds is to be expected. The exact mechanisms driving the increased salinity and temperatures at the surface and the sea ice loss are explored in the next section.

3.3 The Role of the Winds

All the ensemble members are forced with the same wind stress anomalies; therefore, any changes consistently observed across all the members, as seen for the EWS sector, can be attributed to wind-driven processes. The wind stress anomalies can impact the vertical exchanges in the ocean in two main ways.

Firstly, the perturbations modify the wind stress curl (WSC, a measure of the local rotation of the wind), affecting the vertical velocity in the ocean through Ekman transport and mass conservation. In the Southern Hemisphere, a positive (i.e., counter-clockwise) WSC indicates a convergence and causes an Ekman downwelling. The surface waters at high latitudes are generally colder and fresher than the subsurface waters. As most of the Southern Ocean, particularly the EWS, is a region of Ekman upwelling (annual mean state, Supplementary Figure 8), the anomalous positive WSC observed from 1960 to the late 1970s indicates a weakened upwelling. The weakened upwelling may have contributed to the lower surface temperature at that time, and then to the increase of SIE for over a decade during the late 1970s (Figure 5a). In the late 1970s, the WSC over the ESW sector became anomalously negative (Figure 6), driving a stronger Ekman upwelling. The upwelled waters bring salts and warmer waters from the subsurface to the surface, contributing to the loss of SIE, the increase in surface temperature, and salinity during the same period.

The second impact of the imposed wind anomalies is through their influence on vertical mixing, along with a larger wind stress magnitude, inducing a deeper mixed layer and the entrainment of warmer and saltier water at depth in the mixed layer. In the 1960s till the end of the 1970s, the winds were weaker (anomalously negative magnitude) and then shifted to a stronger phase. This drove a stronger vertical mixing, increasing the surface temperature and salinity at the same time as the decrease in SIE.

The combined effects of these two wind-driven mechanisms force a deepening of the mixed layer, a warming and salinification of the surface and a decrease in the SIE in most of the Southern Ocean and specifically the large sea ice loss in the EWS sector. However, the contribution of those two effects cannot be separated in our experiments. The upwelling modified the stratification of the water column and is likely responsible for the positive salinity trend starting at the end of the 1970s. The higher magnitude of the wind stress at the end of the 1970s triggered deeper mixing and a net salt input from below in the surface layer, increasing the surface density and favouring a deep mixed layer in the following years. At the same time, this larger mixing induced a large temperature decrease at depth between the late 1970s and the 1980s, providing part of the heat required to reduce the SIE at that time, with the heat input from a larger upwelling partly compensating for this oceanic heat loss.

4. Conclusion

In this study, we examine the impact of wind changes on the loss of SIE in the Southern Ocean at the end of the 1970s. We use the Earth system model, EC-Earth to conduct a control run and then impose, in a six-member ensemble of sensitivity experiments, wind stress monthly anomalies derived from the ERA5 reanalysis. All 6 ensemble members are initialised at different ocean states and run with constant pre-industrial CO2, to separate the anthropogenic influences. Our results from all the ensemble members unanimously confirm that the sea ice loss at the end of the 1970s was driven by the wind stress perturbation, although the magnitudes differ across different regions. The strengthened wind stress and larger wind stress curl at that time drive a larger upwelling, stronger vertical mixing, warming the surface and decreasing the SIE.

Many factors can influence the evolution of the SIE, but our results indicate that changes in vertical exchanges in the ocean alone can be responsible for major modifications in the SIE. The changes in atmospheric circulation explain the imposed wind stress perturbation in our experiments, and the atmosphere sets the timing of the events. Nevertheless, the initial energy at the origin of the SIE

decrease comes from the ocean, not from the atmosphere. Of course, when the temperature perturbation reaches the surface and the SIE is modified, the positive feedback with the atmosphere can amplify and sustain the response, but this comes only in a second step.

Finally, while our sensitivity experiments suggest a mechanistic causal relationship between the dynamical wind forcing and the sea ice decline, the corresponding mechanism in the real system may involve additional processes. Our experiment design is highly idealised and does not include many elements important for the SIE, such as changes in large-scale atmospheric heat transport, teleconnections from the tropics, and modification of freshwater fluxes towards the Southern Ocean. We thus cannot reproduce the exact details of the interannual variability of the observed SIE extent. The simulated decrease in sea ice extent at the end of the 1970s is also similar to the reconstructions, including its spatial pattern. However, the decrease is larger and less abrupt in our simulations.

The sea ice loss at the end of the 1970s obtained in our simulations can be compared with the SIE shift after 2015 by considering the possible contribution from anthropogenic factors, which we have not discussed here. The wind anomalies have some similarities between the two periods, with larger wind-driven mixing and upwelling around 2015 (Figure 5a), which has likely contributed to the SIE extent drop at that time (Meehl et al., 2019; Spira et al., 2025). Another major common feature is the increase in salinity at the surface since 2015 as shown in recent satellite observations, contradicting the expected freshening due to melting sea ice (Silvano et al., 2025). Our analysis also shows a salinification at the surface towards the end of the 1970s (Figure 5), and similar mechanisms may be at play in both periods.

On the other hand, a noticeable difference between the 1970s sea ice loss and the recent events is in the subsurface temperatures. The ocean temperatures from 100 to 500 metres have warmed in recent years, which has become one of the factors contributing to the sea ice loss along with other atmospheric factors (Zhang et al., 2022). This is in contrast to our studies, where the subsurface has cooled during the sea ice loss. This difference may also explain why in our simulations, the sea ice loss in 2015 is smaller than the one at the end of the 1970s.

This study demonstrates that, even in the absence of atmospheric warming or changes in radiative forcing, and thus no imposed change in heat fluxes from the atmosphere, oceanic changes driven by wind stress anomalies can lead to significant changes in sea ice. The ocean is thus not just a passive player in SIE changes but can play an active role. Further investigating the influence of winds in

different regions of the Southern Ocean and how the ocean responds to them would be beneficial for a better understanding of past and future changes in SIE.

Acknowledgments

This work was performed in the framework of the PDR project T.0101.22 “Role of WINDS and oceanic interactions on Sea ice Changes in the SOuthern Ocean over the Past millennium (WindSCOOP)” of the FRS-FNRS. FF is a postdoctoral fellow supported by the same project. HG is a Research Director within the F.R.S.-FNRS (Belgium). FM is a F.R.S.-FNRS Research Associate (Belgium). Computational resources have been provided by the supercomputing facilities of the Université catholique de Louvain (CISM/UCLouvain) and the Consortium des Equipements de Calcul Intensif en Fédération Wallonie Bruxelles (CECI) funded by F.R.S.-FNRS under convention 2.5020.11 and by the Walloon Region.

References

1. Abram, N. J., Purich, A., England, M. H., McCormack, F. S., Strugnell, J. M., Bergstrom, D. M., Vance, T. R., Stål, T., Wienecke, B., Heil, P., Doddridge, E. W., Sallée, J., Williams, T. J., Reading, A. M., Mackintosh, A., Reese, R., Winkelmann, R., Klose, A. K., Boyd, P. W., . . . Robinson, S. A. (2025). Emerging evidence of abrupt changes in the Antarctic environment. *Nature*, *644*(8077), 621-633. https://doi.org/10.1038/s41586-025-09349-5
2. Armour, K. C., Marshall, J., Scott, J. R., Donohoe, A., & Newsom, E. R. (2016). Southern Ocean warming delayed by circumpolar upwelling and equatorward transport. Nature Geoscience, 9(7), 549–554. https://doi.org/10.1038/ngeo2731
3. Blanchard-Wrigglesworth, E., Roach, L. A., Donohoe, A. & Ding, Q. Impact of winds and Southern Ocean SSTs on Antarctic sea ice trends and variability. J. Clim. 34, 1–47 (2021). https://doi.org/10.1175/JCLI-D-20-0386.1
4. Dalaiden, Q., Abram, N. J., Goosse, H., Holland, P. R., & Topál, D. (2024). Multi-Decadal Variability of Amundsen Sea Low Controlled by Natural Tropical and Anthropogenic Drivers. Geophysical Research Letters, 51(16), e2024GL109137. https://doi.org/10.1029/2024GL109137
5. Dalaiden, Q., Goosse, H., Rezsöhazy, J. et al. Reconstructing atmospheric circulation and sea-ice extent in the West Antarctic over the past 200 years using data assimilation. Clim Dyn 57, 3479–3503 (2021). https://doi.org/10.1007/s00382-021-05879-6

6. de la Mare, W.K. Changes in Antarctic sea-ice extent from direct historical observations and whaling records. Climatic Change 92, 461–493 (2009). https://doi.org/10.1007/s10584-008-9473-2

7. DiGirolamo, N. E., C. L. Parkinson, D. J. Cavalieri, P. Gloersen, and H. J. Zwally. 2022, updated yearly. Sea Ice Concentrations from Nimbus-7 SMMR and DMSP SSM/I-SSMIS Passive Microwave Data, Version 2. Boulder, Colorado USA. NASA National Snow and Ice Data Center Distributed Active Archive Center. https://doi.org/10.5067/MPYG15WAA4WX.

8. Döscher, R., Acosta, M., Alessandri, A., Anthoni, P., Arsouze, T., Bergman, T., Bernardello, R., Boussetta, S., Caron, L.-P., Carver, G., Castrilllso, M., Catalano, F., Cvijanovic, I., Davini, P., Dekker, E., Doblas-Reyes, F. J., Docquier, D., Echevarria, P., Fladrich, U., Fuentes-Franco, R., Gröger, M., v. Hardenberg, J., Hieronymus, J., Karami, M. P., Keskinen, J.-P., Koenigk, T., Makkonen, R., Massonnet, F., Ménégoz, M., Miller, P. A., Moreno-Chamarro, E., Nieradzik, L., van Noije, T., Nolan, P., O'Donnell, D., Ollinaho, P., van den Oord, G., Ortega, P., Prims, O. T., Ramos, A., Reerink, T., Rousset, C., Ruprich-Robert, Y., Le Sager, P., Schmith, T., Schrödner, R., Serva, F., Sicardi, V., Sloth Madsen, M., Smith, B., Tian, T., Tourigny, E., Uotila, P., Vancoppenolle, M., Wang, S., Wårlind, D., Willén, U., Wyser, K., Yang, S., Yepes-Arbós, X., and Zhang, Q.: The EC-Earth3 Earth system model for the Coupled Model Intercomparison Project 6, Geosci. Model Dev., 15, 2973–3020, https://doi.org/10.5194/gmd-15-2973-2022, 2022

9. Espinosa, Z. I., E. Blanchard-Wrigglesworth, and C. M. Bitz, 2024: Understanding the drivers and predictability of record low Antarctic sea ice in austral winter 2023. Communications Earth & Environment, 5, 723, https://doi.org/10.1038/s43247-024-01772-2.

10. Eyring, V., Bony, S., Meehl, G. A., Senior, C. A., Stevens, B., Stouffer, R. J., and Taylor, K. E.: Overview of the Coupled Model Intercomparison Project Phase 6 (CMIP6) experimental design and organization, Geosci. Model Dev., 9, 1937–1958, https://doi.org/10.5194/gmd-9-1937-2016, 2016

11. Fogt, R.L., Sleinkofer, A.M., Raphael, M.N. et al. (2022). A regime shift in seasonal total Antarctic sea ice extent in the twentieth century. Nat. Clim. Chang. 12, 54–62. https://doi.org/10.1038/s41558-021-01254-9

12. Goosse, H., Dalaiden, Q., Feba, F. *et al.* A drop in Antarctic sea ice extent at the end of the 1970s. *Commun Earth Environ* **5**, 628 (2024). https://doi.org/10.1038/s43247-024-01793-x

13. Goosse, H., & Fichefet, T. (1999). Importance of ice-ocean interactions for the global ocean circulation: A model study. *Journal of Geophysical Research: Oceans*, *104*(C10), 23337–23355. https://doi.org/10.1029/1999JC900215

14. Hersbach, H., Bell, B., Berrisford, P., Biavati, G., Horányi, A., Muñoz Sabater, J., Nicolas, J., Peubey, C., Radu, R., Rozum, I., Schepers, D., Simmons, A., Soci, C., Dee, D., Thépaut, J-N. (2023): ERA5 hourly data on single levels from 1940 to present. Copernicus Climate Change Service (C3S) Climate Data Store (CDS), https://doi.org/10.24381/cds.adbb2d47

15. Himmich, K., Vancoppenolle, M., Stammerjohn, S., Bocquet, M., Madec, G., Sallée, B., & Fleury, S. (2024). Thermodynamics Drive Post-2016 Changes in the Antarctic Sea Ice Seasonal Cycle. Journal of Geophysical Research: Oceans, 129(8), e2024JC021112. https://doi.org/10.1029/2024JC021112

16. Hobbs, W., Spence, P., Meyer, A., Schroeter, S., Fraser, A., Reid, P., Tian, T., Wang, Z., Liniger, G., Doddridge, E. and Boyd, P. (2024). Observational Evidence for a Regime Shift in Summer Antarctic Sea Ice. *Journal of Climate* 37(7) pp. 2263-2275. https://doi.org/10.1175/JCLI-D-23-0479.1

17. Hobbs, W. R., Massom, R., Stammerjohn, S., Reid, P., Williams, G., & Meier, W. (2016). A review of recent changes in Southern Ocean sea ice, their drivers and forcings. Global anwd Planetary Change, 143, 228–250. https://doi.org/10.1016/j.gloplacha.2016.06.008

18. Holland, P. R., & Kwok, R. (2012). Wind-driven trends in Antarctic sea-ice drift. Nature Geoscience, 5(12), 872-875. https://doi.org/10.1038/ngeo1627

19. Hosking, J. S., A. Orr, G. J. Marshall, J. Turner, and T. Phillips, 2013: The Influence of the Amundsen–Bellingshausen Seas Low on the Climate of West Antarctica and Its Representation in Coupled Climate Model Simulations. J. Climate, 26, 6633–6648, https://doi.org/10.1175/JCLI-D-12-00813.1.

20. Jena, B., S. Kshitija, C. Bajish, J. Turner, C. Holmes, J. Wilkinson, R. Mohan, and M. Thamban, 2024: Evolution of Antarctic sea ice ahead of the record low annual maximum extent in September 2023. Geophys Res Lett, 51, e2023GL107561, https://doi.org/10.1029/2023GL107561

21. Lecomte, O., Goosse, H., Fichefet, T. et al. Vertical ocean heat redistribution sustaining sea-ice concentration trends in the Ross Sea. Nat Commun 8, 258 (2017). https://doi.org/10.1038/s41467-017-00347-4

22. Lefebvre, W., and H. Goosse (2008), An analysis of the atmospheric processes driving the large-scale winter sea ice variability in the Southern Ocean, *J. Geophys. Res.*, 113, C02004, https://doi.org/10.1029/2006JC004032

23. Madec, G.: NEMO ocean engine, Note du Pole de modelisation de l'Institut Pierre-Simon Laplace No 27, ISSN No 1288-1619, 2015

24. Massom, R. A., S. E. Stammerjohn, W. Lefebvre, S. A. Harangozo, N. Adams, T. A. Scambos, M. J. Pook, and C. Fowler (2008), West Antarctic Peninsula sea ice in 2005: Extreme ice compaction and ice edge retreat due to strong anomaly with respect to climate, J. Geophys. Res., 113, C02S20, https://doi.org/10.1029/2007JC004239

25. Matear, R., O'Kane, T., Risbey, J. et al. Sources of heterogeneous variability and trends in Antarctic sea-ice. Nat Commun 6, 8656 (2015). https://doi.org/10.1038/ncomms9656

26. Meehl, G.A., Arblaster, J.M., Chung, C.T.Y. *et al.* Sustained ocean changes contributed to sudden Antarctic sea ice retreat in late 2016. *Nat Commun* **10**, 14 (2019). https://doi.org/10.1038/s41467-018-07865-9

27. Parkinson, C.L., 2019. A 40-y record reveals gradual Antarctic sea ice increases followed by decreases at rates far exceeding the rates seen in the Arctic. Proc. Nat. Acad. Sci. (PNAS) 116 (29), 14,414–14,423

28. Purich, A., and M. H. England, 2019: Tropical teleconnections to Antarctic sea ice during austral spring 2016 in coupled pacemaker experiments. Geophys. Res. Lett., 46, 6848–6858, https://doi.org/10.1029/2019GL082671.

29. Purich, A., and E. W. Doddridge, 2023: Record low Antarctic sea ice coverage indicates a new sea ice state. Communications Earth & Environment, 4(1), 314, https://doi.org/10.1038/s43247-023-00961-9.

30. Raphael, M. N. The influence of atmospheric zonal wave three on Antarctic sea ice variability. J. Geophys. Res. 112, 2006JD007852 (2007) https://doi.org/10.1029/2006JD007852

31. Raphael, M. N., and W. Hobbs (2014), The influence of the large-scale atmospheric circulation on Antarctic sea ice during ice advance and retreat seasons, Geophys. Res. Lett., 41, 5037–5045, https://doi.org/10.1002/2014GL060365.

32. Raphael, M.N., Maierhofer, T.J., Fogt, R.L. *et al.* A twenty-first century structural change in Antarctica's sea ice system. *Commun Earth Environ* **6**, 131 (2025). https://doi.org/10.1038/s43247-025-02107-5

33. Roach, L. A., Dörr, J., Holmes, C. R., Massonnet, F., Blockley, E. W., Notz, D., Rackow, T., Raphael, M. N., Bailey, D. A., & Bitz, C. M. (2020). Antarctic Sea Ice Area in CMIP6. *Geophysical Research Letters*, *47*(9), e2019GL086729. https://doi.org/10.1029/2019GL086729

34. Roach, L. A. et al. Winds and meltwater together lead to Southern Ocean surface cooling and sea ice expansion. Geophys. Res. Lett. 50, e2023GL105948 (2023). https://doi.org/10.1029/2023GL105948

35. Roach, L.A., Meier, W.N. Sea ice in 2024. *Nat Rev Earth Environ* **6**, 252–254 (2025). https://doi.org/10.1038/s43017-025-00662-1

36. Rousset, C., Vancoppenolle, M., Madec, G., Fichefet, T., Flavoni, S., Barthélemy, A., Benshila, R., Chanut, J., Levy, C., Masson, S., and Vivier, F.: The Louvain-La-Neuve sea ice model LIM3.6: global and regional capabilities, Geosci. Model Dev., 8, 2991–3005, https://doi.org/10.5194/gmd-8-2991-2015, 2015

37. Rintoul, S.R. The global influence of localized dynamics in the Southern Ocean. *Nature* **558**, 209–218 (2018). https://doi.org/10.1038/s41586-018-0182-3

38. Schlosser, E., Alexander Haumann, F., Raphael, M. N., Haumann, F. A. & Raphael, M. N. Atmospheric influences on the anomalous 2016 Antarctic sea ice decay. Cryosphere 12, 1103–1119 (2018). https://doi.org/10.5194/tc-12-1103-2018

39. Schroeter, S. (2025). Seasonal and Regional Antarctic Sea Ice Biases: A Closer Look at CMIP6. Atmosphere-Ocean, 1–18. https://doi.org/10.1080/07055900.2025.2507880

40. A. Silvano, A. Narayanan, R. Catany, E. Olmedo, V. González-Gambau, A. Turiel, R. Sabia, M.R. Mazloff, T. Spira, F.A. Haumann, & A.C. Naveira Garabato (2025), Rising surface salinity and declining sea ice: A new Southern Ocean state revealed by satellites, Proc. Natl. Acad. Sci. U.S.A. 122 (27) e2500440122, https://doi.org/10.1073/pnas.2500440122.

41. Spira, T., Swart, S., Giddy, I. & du Plessis, M. The Observed Spatiotemporal Variability of Antarctic Winter Water. J. Geophys. Res. Oceans 129, e2024JC021017 (2024).

42. Stuecker, M. F., Bitz, C. M., & Armour, K. C. (2017). Conditions leading to the unprecedented low Antarctic sea ice extent during the 2016 austral spring season. Geophysical Research Letters, 44(17), 9008-9019. https://doi.org/10.1002/2017GL074691

43. Thomas, J. L., D. W. Waugh, and A. Gnanadesikan (2015), Southern Hemisphere extratropical circulation: Recent trends and natural variability, *Geophys. Res. Lett.*, 42, 5508–5515, doi:10.1002/2015GL064521

44. Turner, J., T. Phillips, G. J. Marshall, J. S. Hosking, J. O. Pope, T. J. Bracegirdle, and P. Deb (2017), Unprecedented springtime retreat of Antarctic sea ice in 2016, *Geophys. Res. Lett.*, 44, 6868–6875, doi:10.1002/2017GL073656

45. Vancoppenolle, M., Bouillon, S., Fichefet, T., Goosse, H. Lecomte, O., Morales Maqueda, M. A., and Madec, G.: LIM The Louvain-la-Neuve sea Ice Model, Tech. Rep. 31, Note du Pôle de Modélisation de l'Institut Pierre-Simon Laplace No. 31, ISSN No 1288-1619, https://cmc.ipsl.fr/images/publications/scientific_notes/lim3_book.pdf (last access: 24 July 2025), 2012

46. Wang, J., Massonnet, F., Goosse, H. et al. Synergistic atmosphere-ocean-ice influences have driven the 2023 all-time Antarctic sea-ice record low. Commun Earth Environ 5, 415 (2024). https://doi.org/10.1038/s43247-024-01523-3

47. Yang, J., Xiao, C., Liu, J., Li, S., & Qin, D. (2021). Variability of Antarctic sea ice extent over the past 200 years. *Science Bulletin*, *66*(23), 2394-2404. https://doi.org/10.1016/j.scib.2021.07.028

48. Zhang, L., Delworth, T.L., Yang, X. et al. The relative role of the subsurface Southern Ocean in driving negative Antarctic Sea ice extent anomalies in 2016–2021. Commun Earth Environ 3, 302 (2022). https://doi.org/10.1038/s43247-022-00624-1

49. Zhou, S., Meijers, A. J., Meredith, M. P., Abrahamsen, E. P., Holland, P. R., Silvano, A., Sallée, J., & Østerhus, S. (2023). Slowdown of Antarctic Bottom Water export driven by climatic wind and sea-ice changes. *Nature Climate Change*, *13*(7), 701-709. https://doi.org/10.1038/s41558-023-01695-4

Figures

Fig 1) The evolution of the sea ice extent (SIE) anomalies from the EC-Earth simulations, in different Sectors of the Southern Ocean. The dotted red line represents the control run (EC-CTL), the black line indicates the ensemble mean (EnsMean), and each of the other lines represents one of the six wind-stress-forced realisations (ECN1-ECN6). The anomalies are calculated with the baseline 1960-2022.

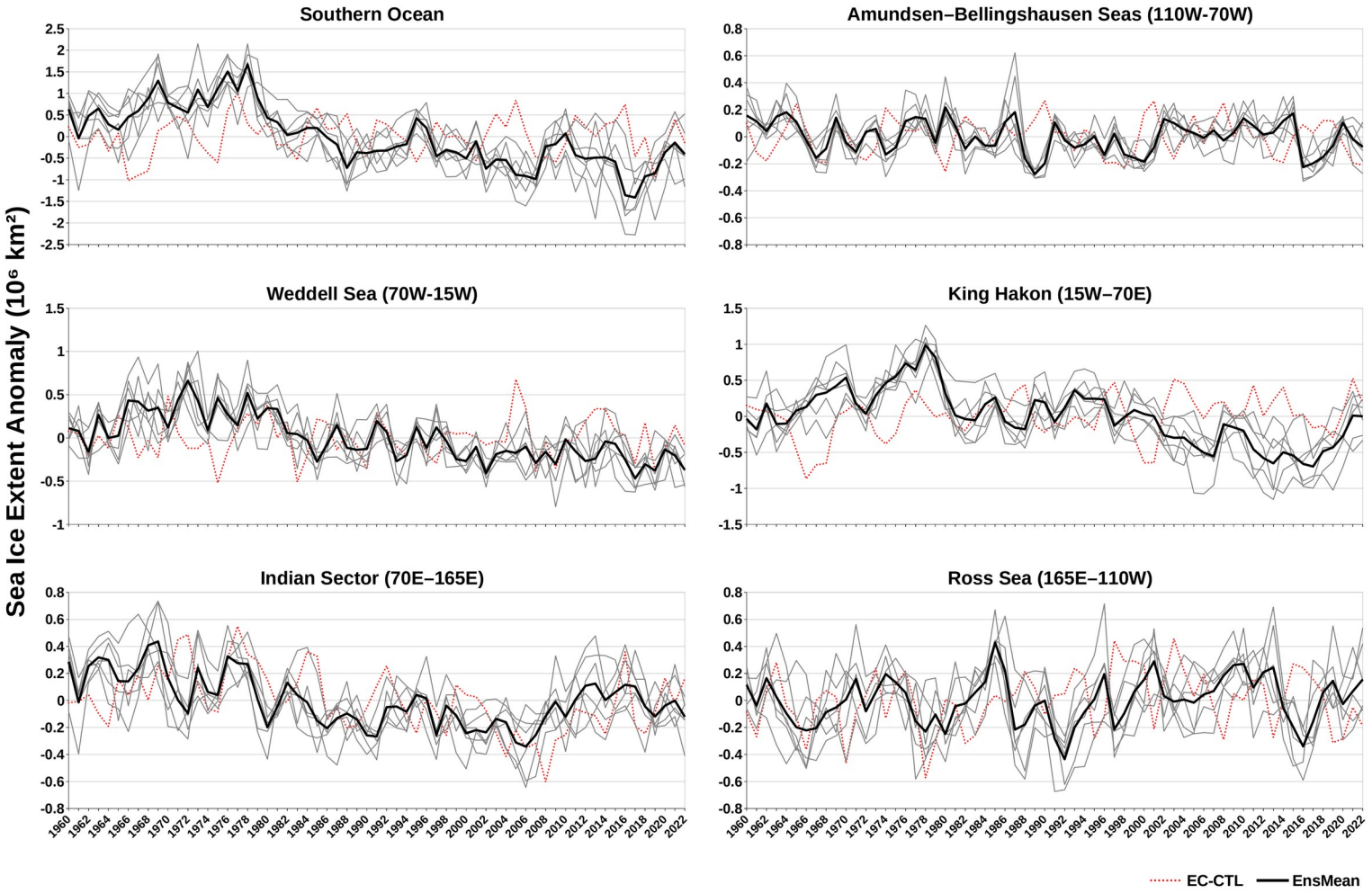

Fig 2) The difference in sea ice concentration (SIC) between the post-loss period (1990-1994) and the pre-loss period (1976-1980) from the ensemble mean (EnsMean). The regions at 5% significance are hatched.

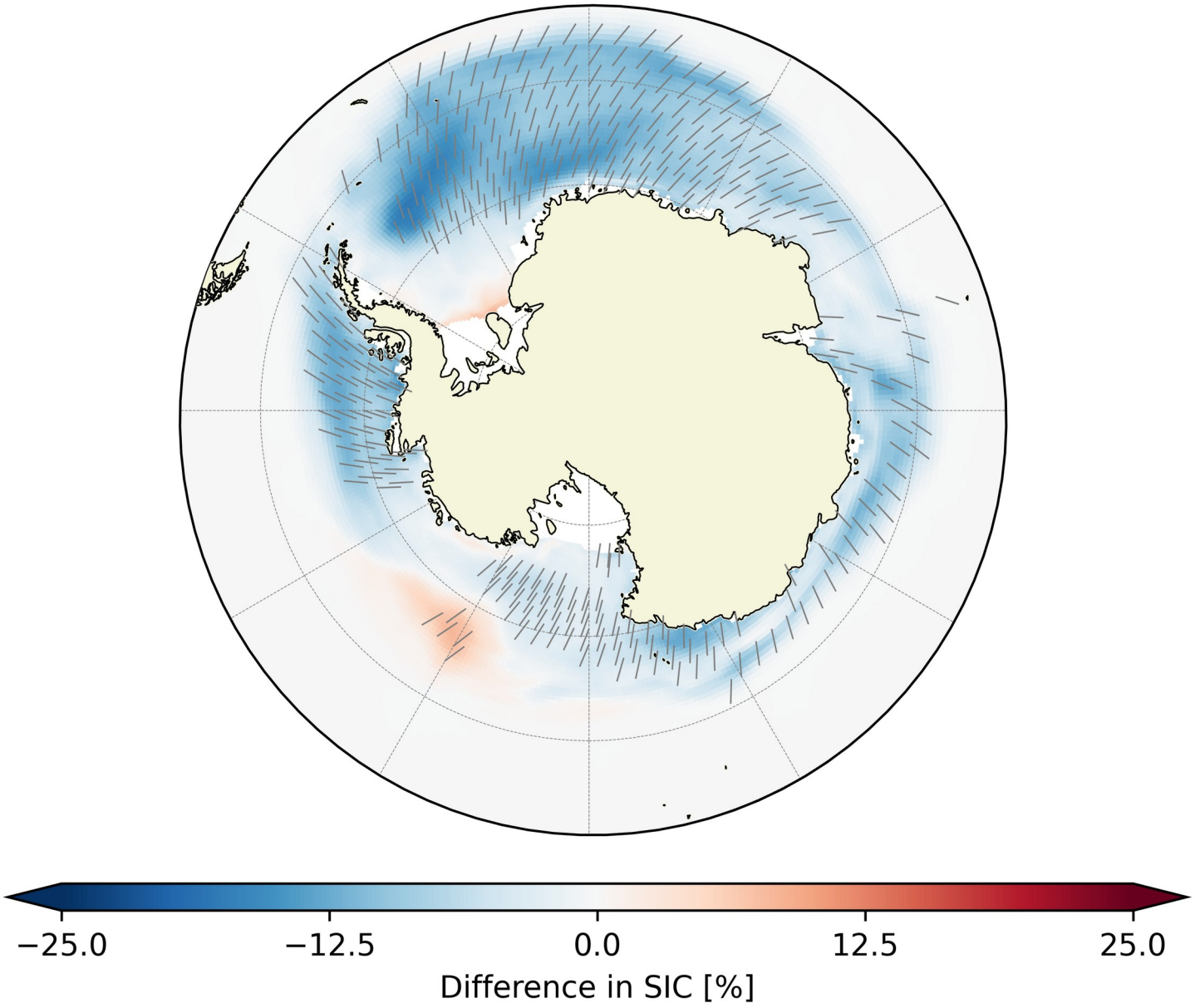

Fig 3) The difference in ocean temperatures between the post-loss period (1990-1994) and the pre-loss period (1976-1980) from the ensemble mean (EnsMean). a) Sea surface temperature (SST); Ocean temperatures b) from surface to 100m depth and c) from 100m to 500m depth.

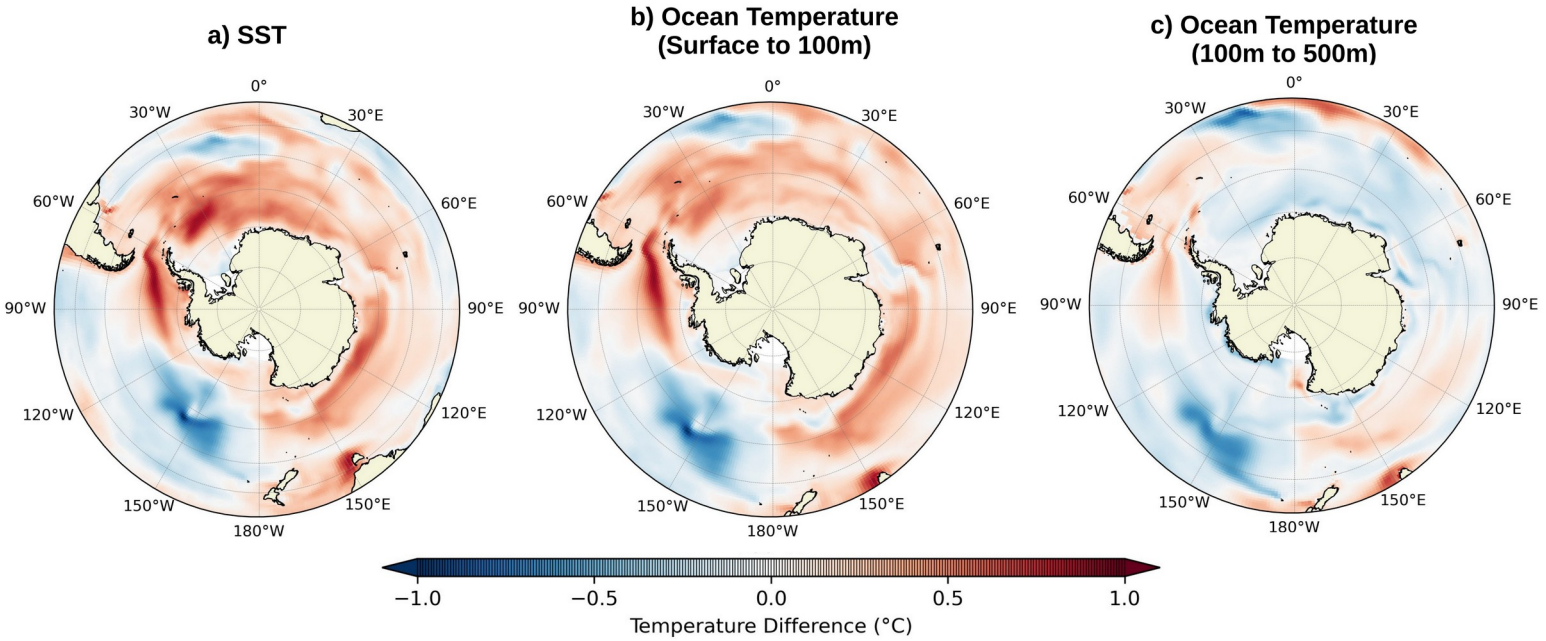

Fig 4) The differences in a) Mixed Layer Depth and b) Vertical Temperature-Salinity profiles, post-loss (1990-1994) and pre-loss (1976-1980) from the ensemble mean over the region with the maximum loss of sea ice.

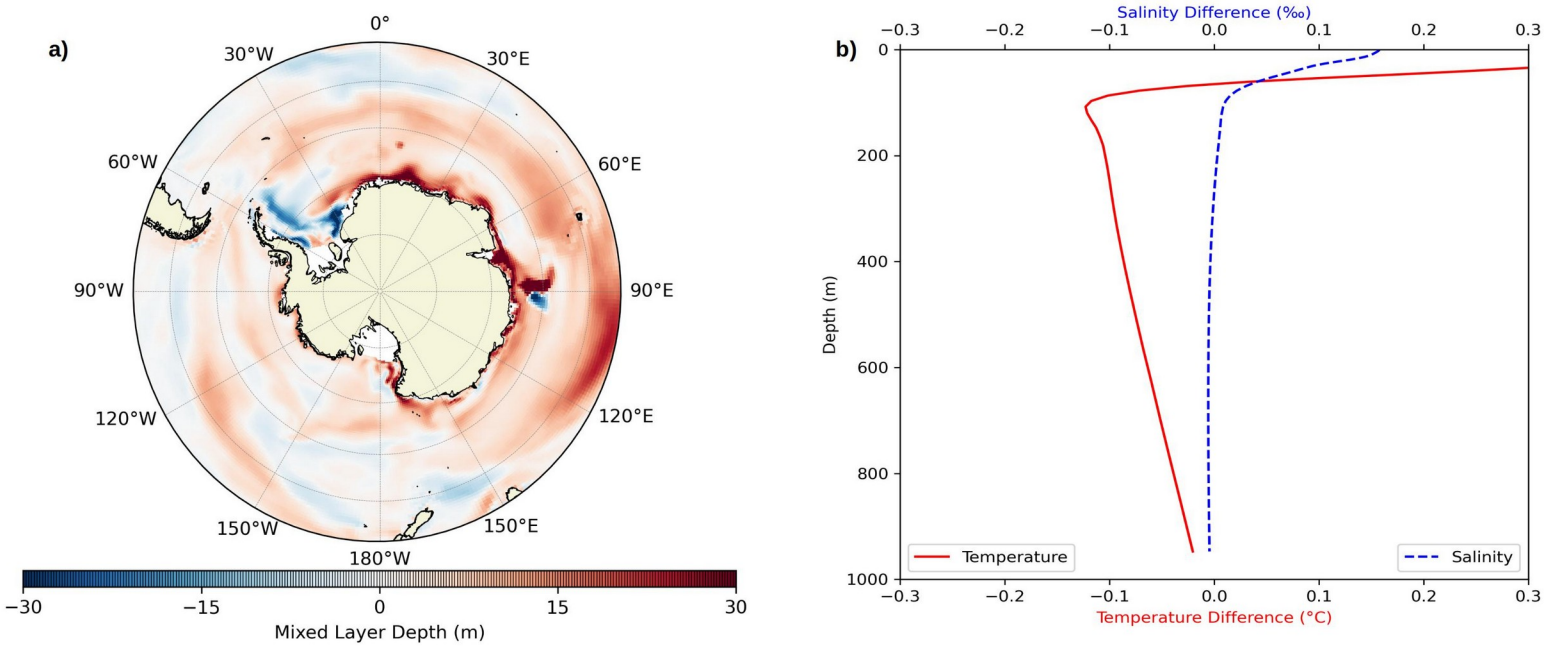

Fig 5) The evolution of the anomalies of a) Wind stress magnitude (N/m2), Wind stress curl (N/m3) and Sea ice extent (Million km2); b) Temperature and salinity from surface to 100m and c) from 100m to 500m depth, averaged over the region with the maximum loss of sea ice, from 55°S to 70°S, 50°W to 30°E. The anomalies are calculated from the ensemble mean with the baseline 1960-2022.

a)

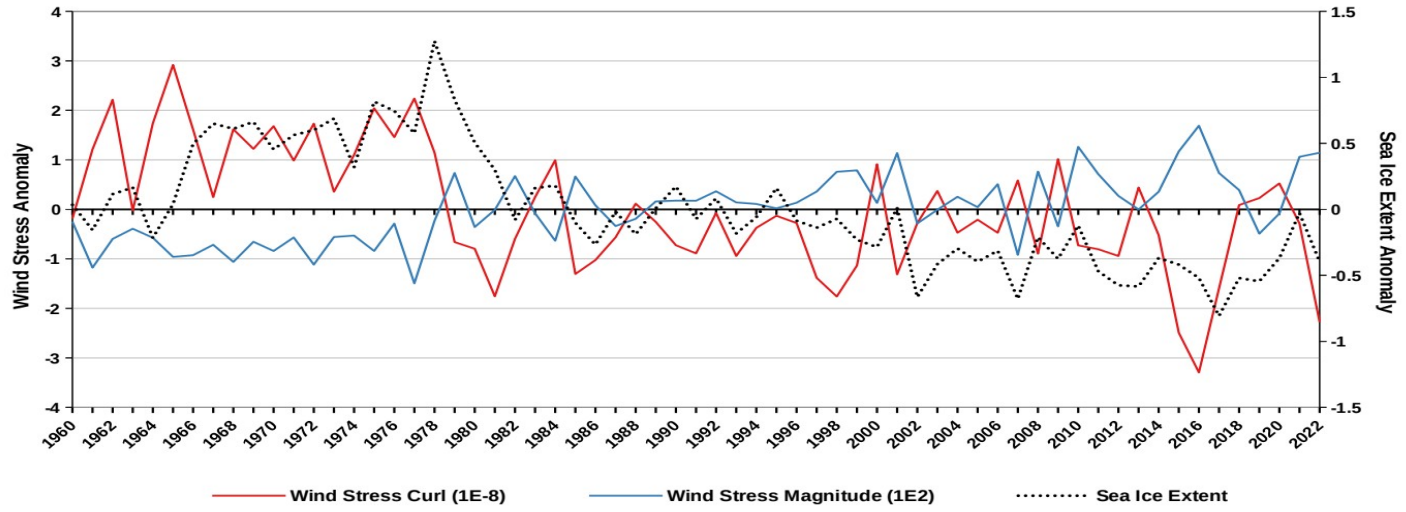
Wind Stress Anomaly
Sea Ice Extent Anomaly
Wind Stress Curl (1E-8)
Wind Stress Magnitude (1E2)
Sea Ice Extent

b)

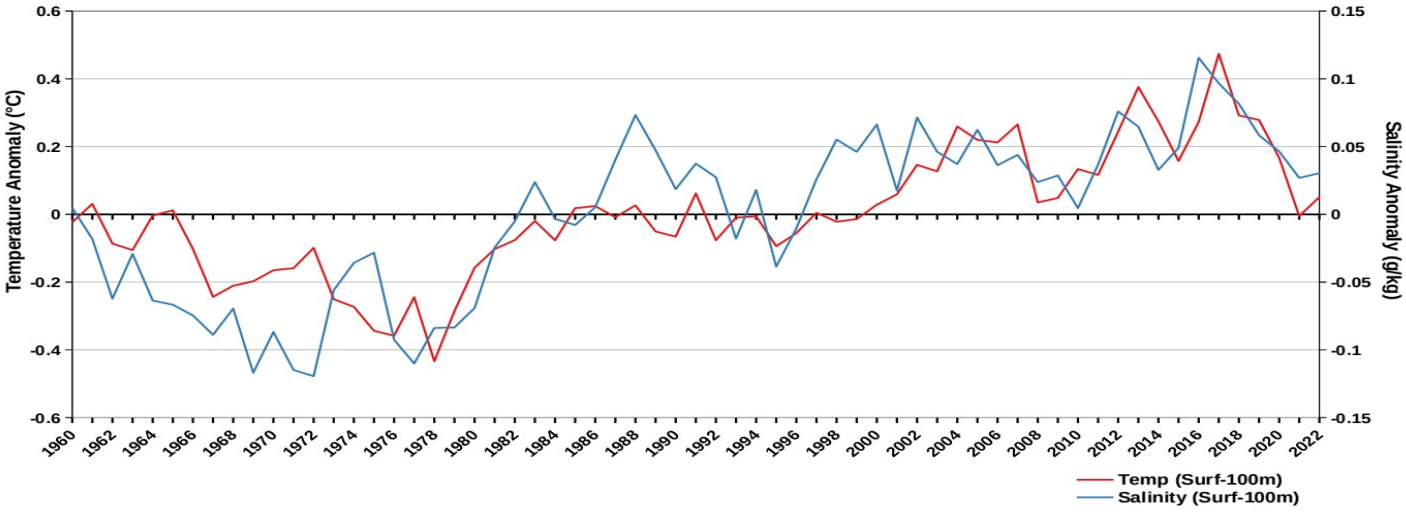
Temperature Anomaly (°C)
Salinity Anomaly (g/kg)
Temp (Surf-100m)
Salinity (Surf-100m)

c)

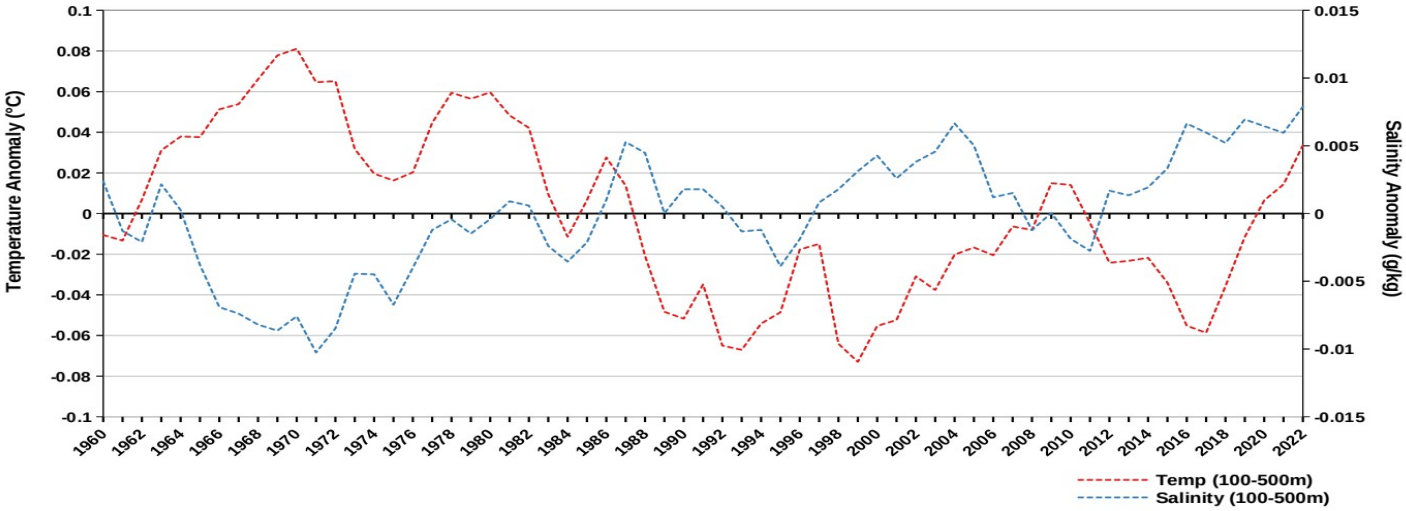
Temperature Anomaly (°C)
Salinity Anomaly (g/kg)
Temp (100-500m)
Salinity (100-500m)

Fig 6) The wind curl difference post-loss (1990-1994) and pre-loss (1976-1980) from the ensemble mean overlaid with the difference in windstress vectors.

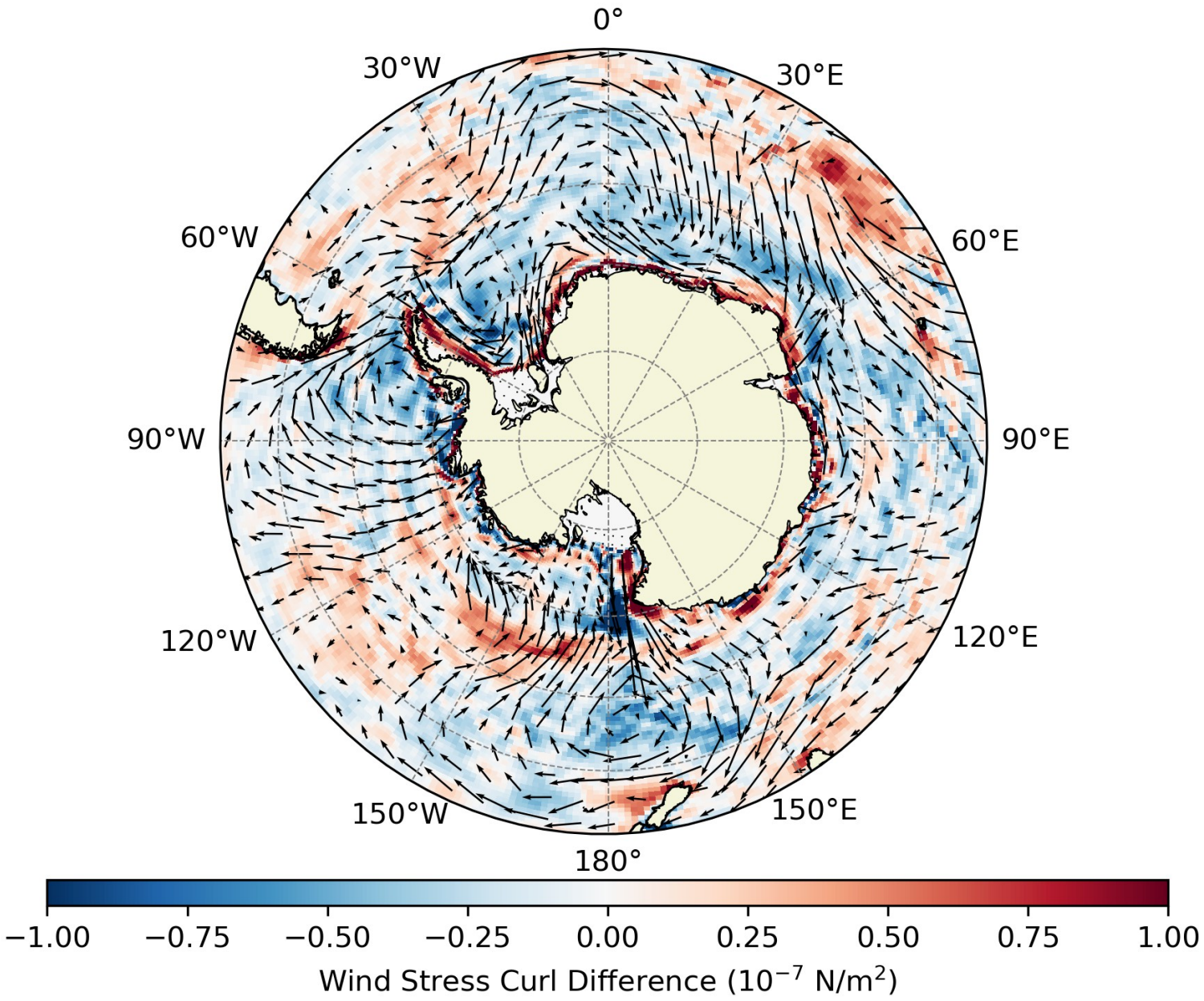

Supplementary Material

S.Figure 1) The sea ice extent (SIE) climatology in the Southern Ocean from the EC-Earth simulations. The monthly climatology is calculated over the period 1979-2022 to be comparable with the NSIDC dataset.

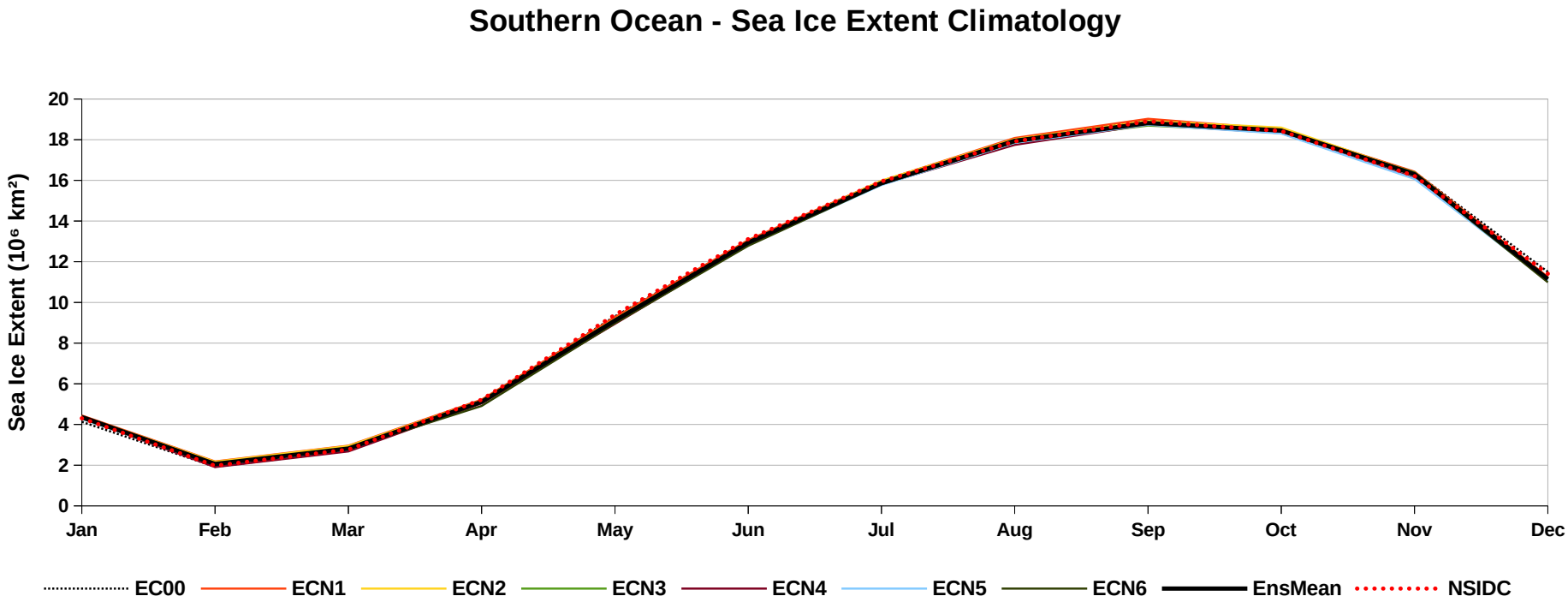

S.Figure 2) The sea ice extent (SIE) in the Southern Ocean from the EC-Earth simulations. The black line indicates the ensemble mean (EnsMean) from the six wind-stress-forced realisations (in grey) with the range of 1 standard deviation shaded. The red line shows the standard deviation (Std-Dev) across the ensemble members on a separate y-axis.

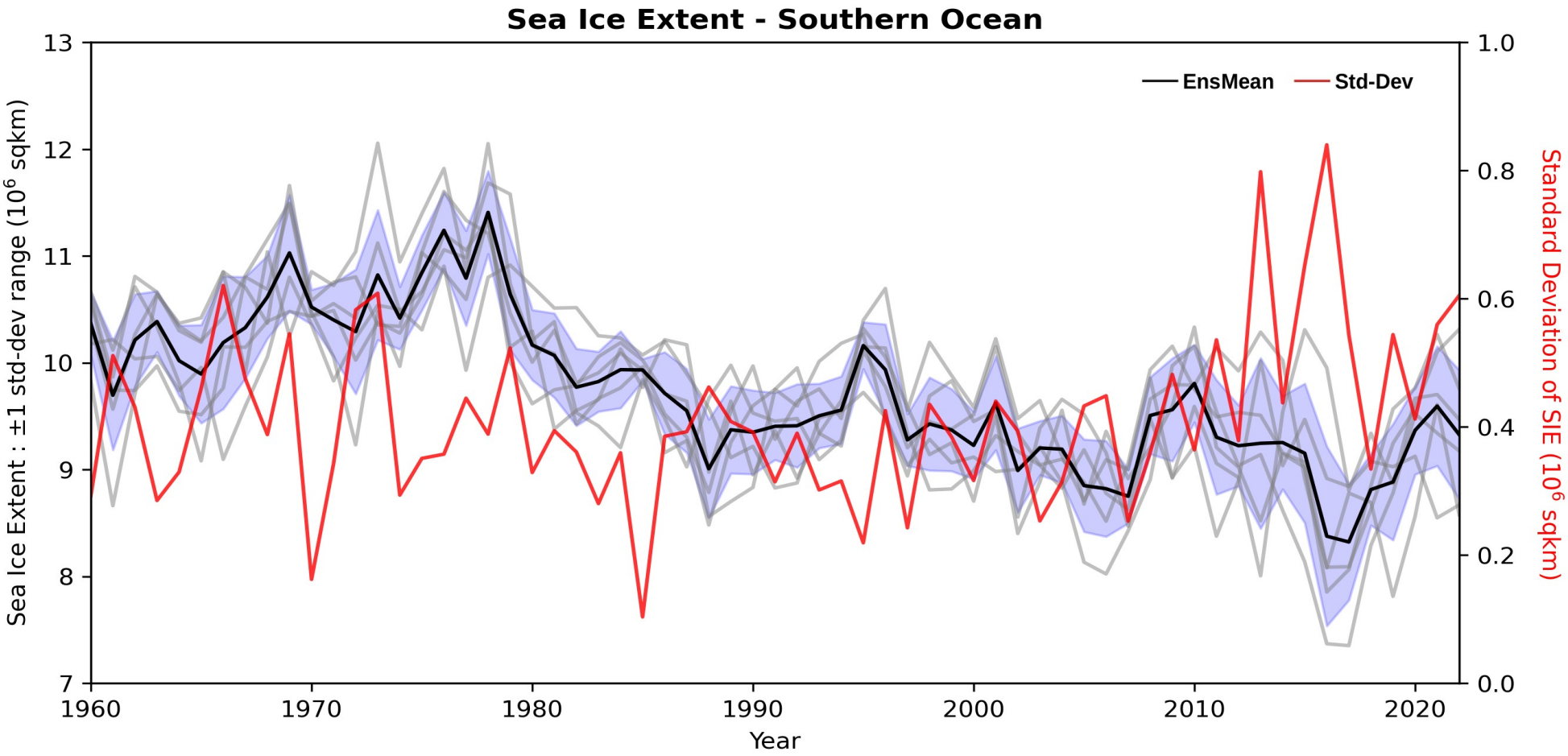

S.Figure 3) The two periods, the period of maximum extent before the loss from 1976 to 1980 (pre-loss), and the subsequent minimum extent from 1990 to 1994 (post-loss) indicating a decrease of 1.28 million km^2 of SIE across the total Southern Ocean.

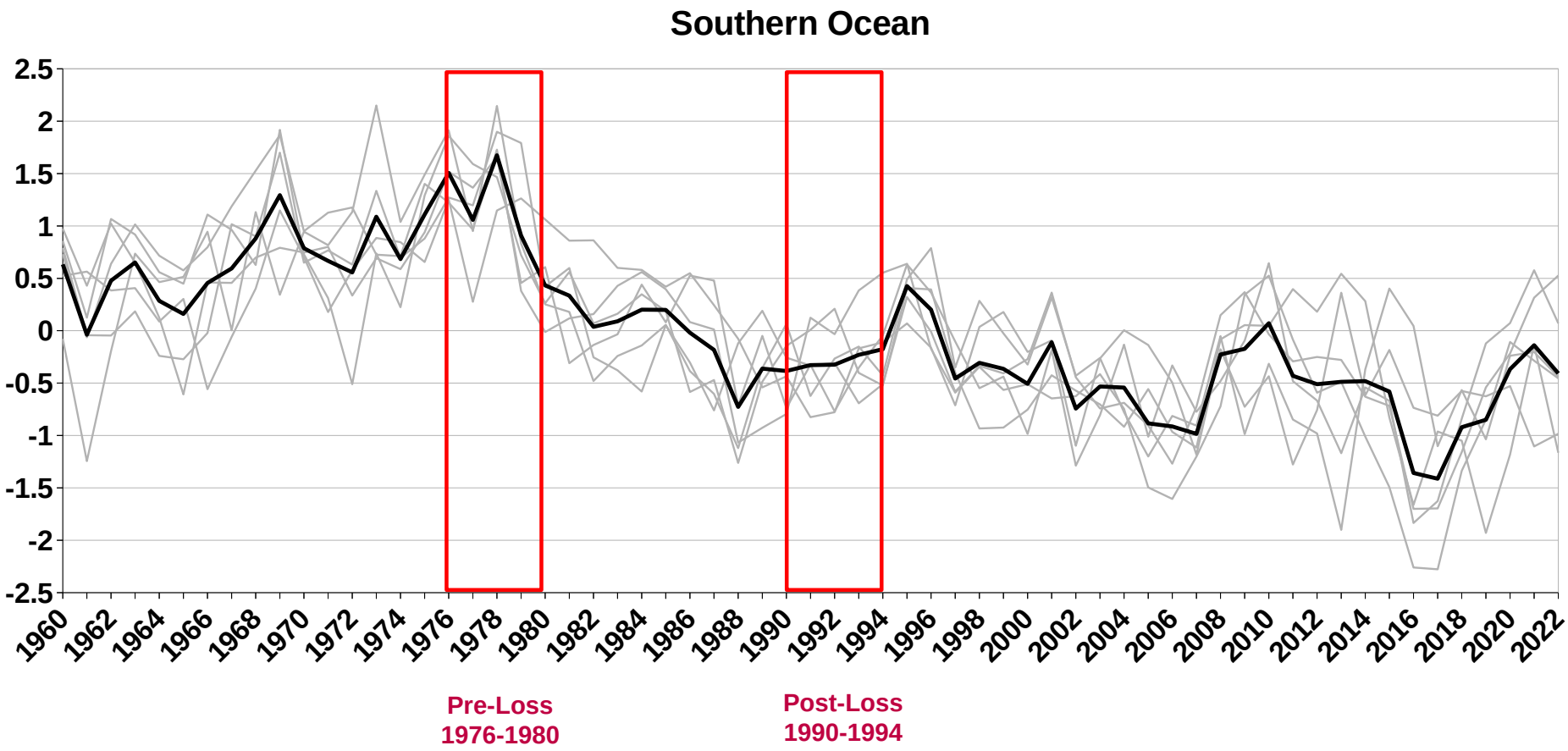

S.Figure 4) The difference in the average of SIE post-loss (1990-1995) and pre-loss (1975-1980). The ensemble members are in agreement that all sectors show a loss of varying magnitude in the total sea ice extent except for the Ross Sea, where the members differ.

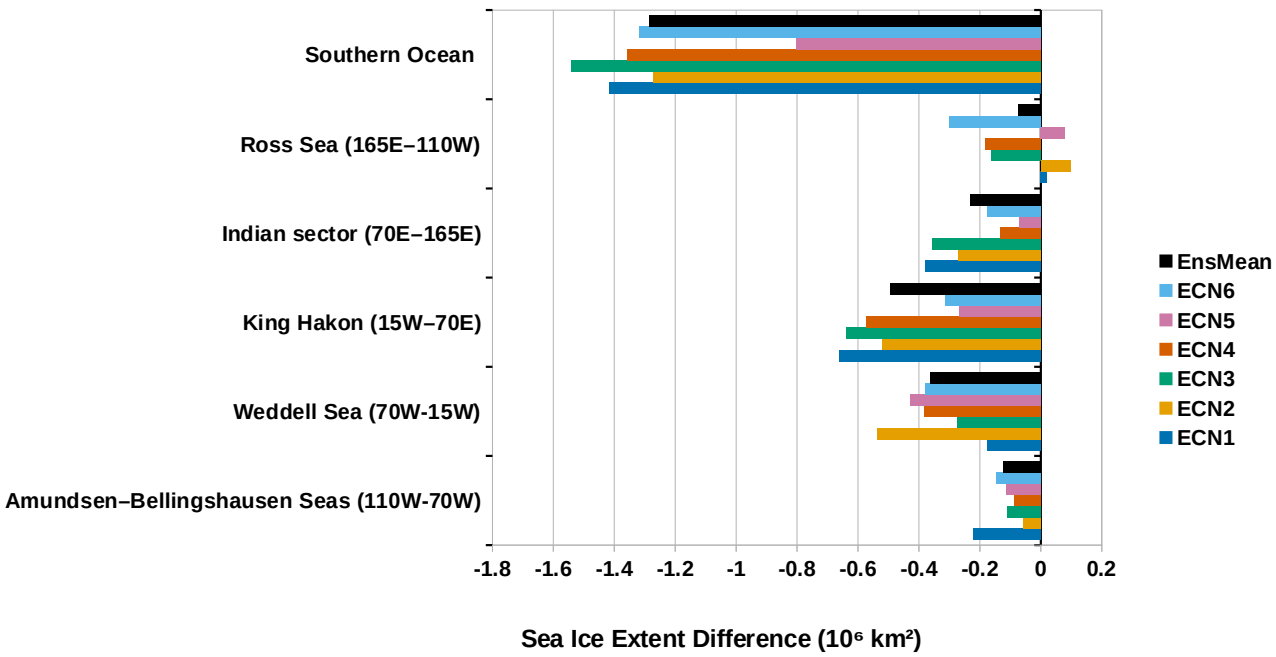

S. Figure 5) The difference in the average of the sea ice concentration (SIC) post-loss (1990-1994) and pre-loss (1976-1980).

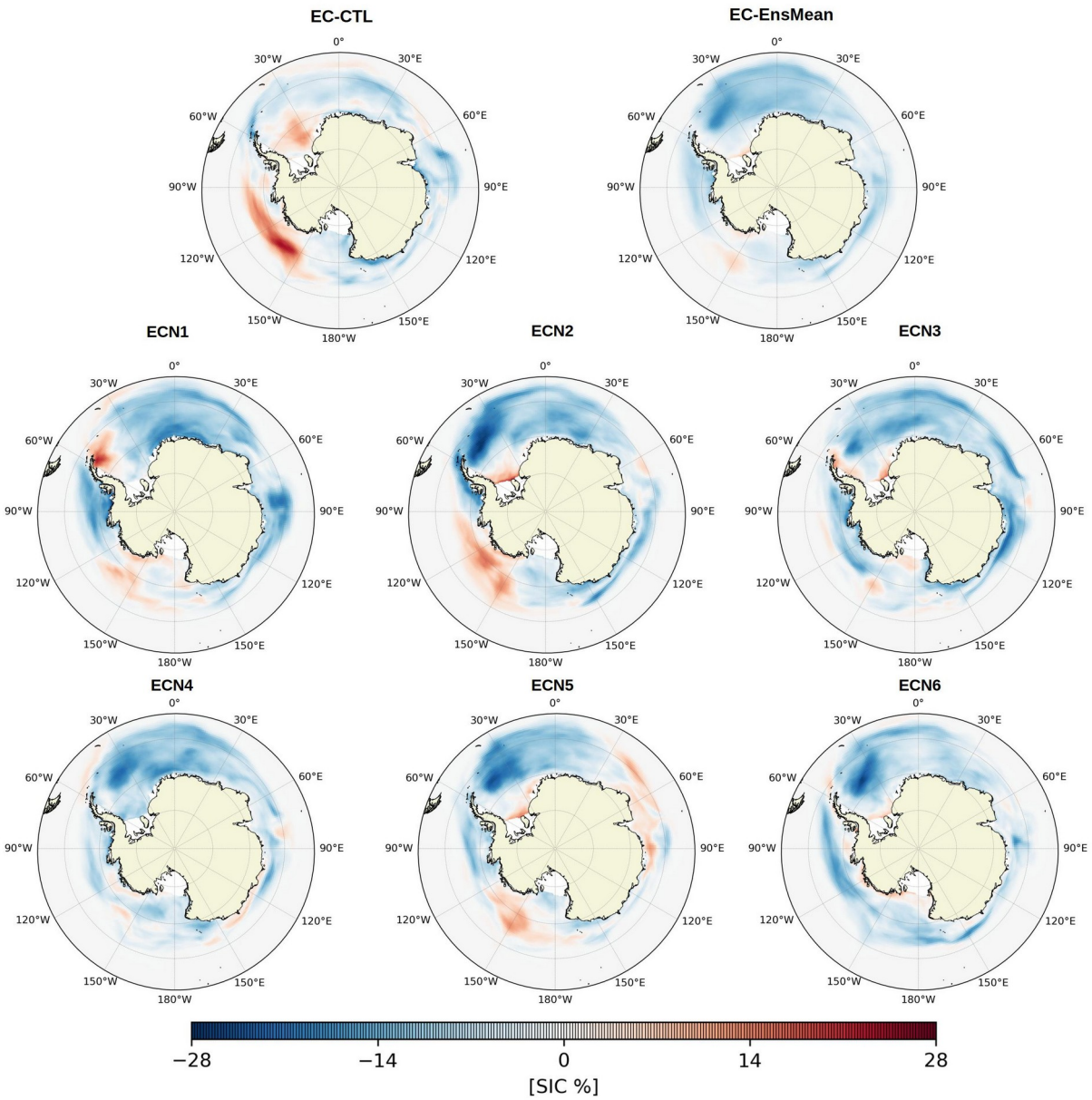

S. Figure 6) The annual mean of mixed layer depth (MLD) annually averaged over the region with the maximum loss of sea ice, from 55°S to 70°S, 50°W to 30°E. The MLD deepens exceedingly (polynyas) in some years post 2000, thereby skewing the anomaly values. Sea ice extent (SIE) anomalies over the same region are overlaid for comparision. The deepening of the MLD coincides with the decrease of SIE in the region during the late 1970s.

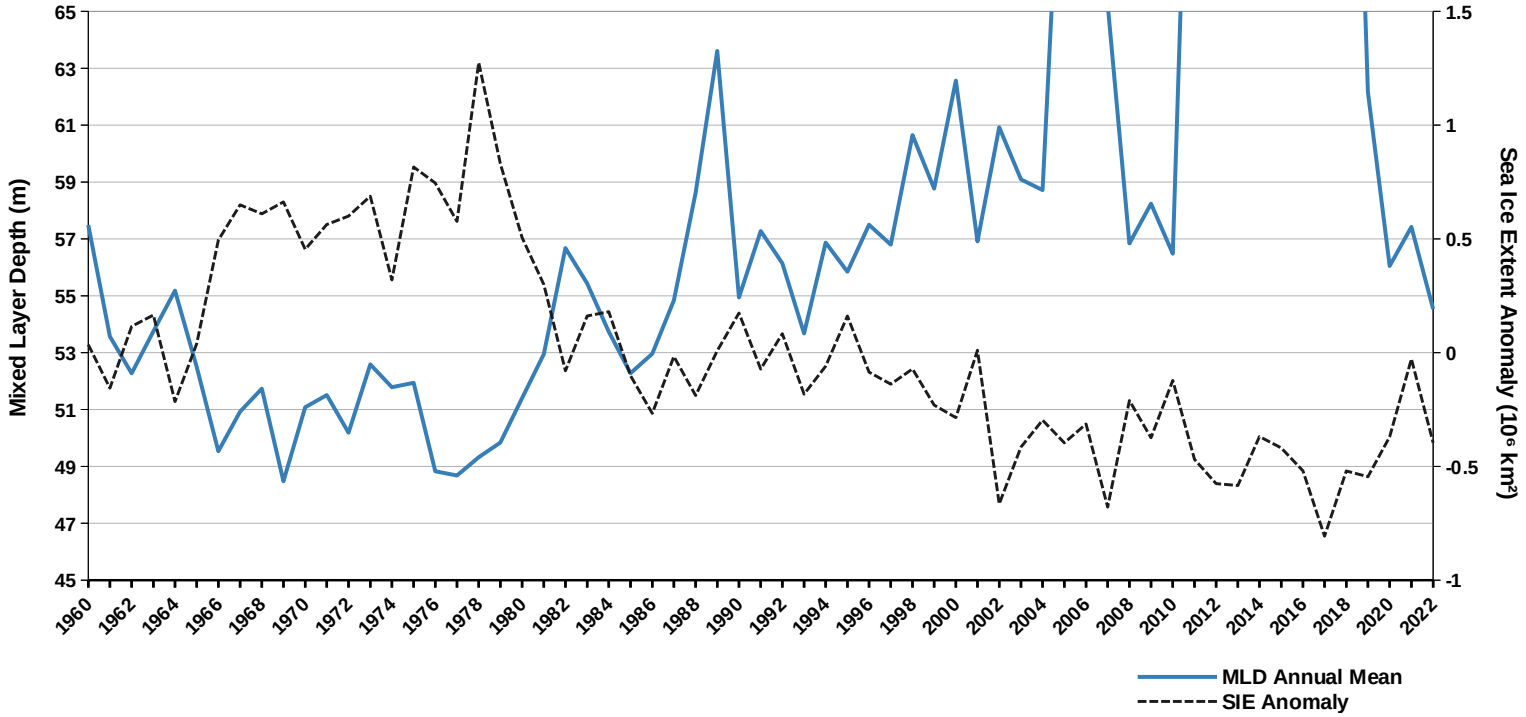

S. Figure 7) The difference in ocean current magnitude between the post-loss period (1990-1994) and the pre-loss period (1976-1980) from the ensemble mean (EnsMean).

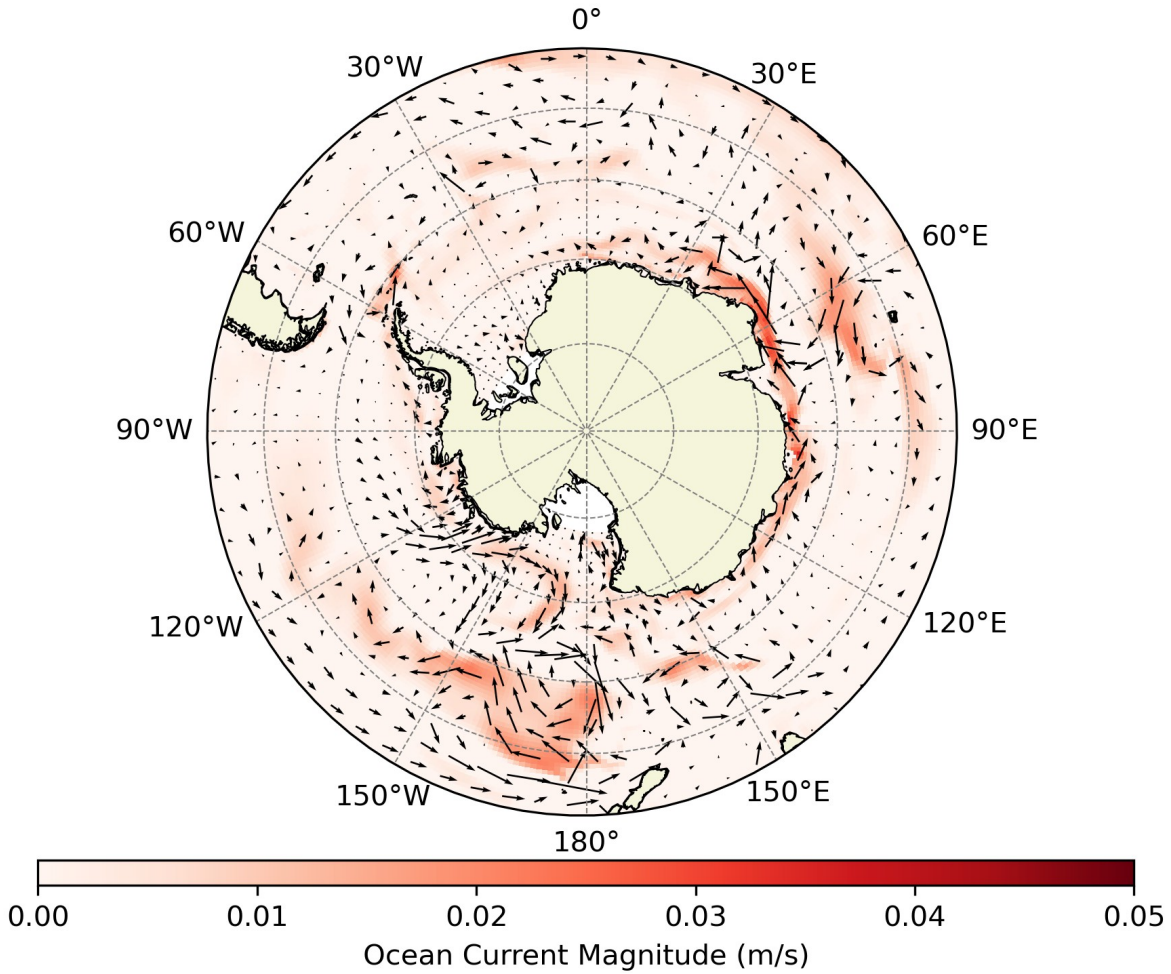

S. Figure 8) The annual mean state of the wind stress curl (WSC) in the Southern Ocean, calculated from the EnsMean, averaging from 1960 to 2022. Note: the colorbar is on a logarithmic scale.